Applied Catalysis B: Environmental 84 (2008) 112–118

Contents lists available at ScienceDirect

Applied Catalysis B: Environmental

journal homepage: www.elsevier.com/locate/apcatb

Pt/titania-nanotube: A potential catalyst for CO_2 adsorption and hydrogenation

Kuo-Pin Yu [a], Wen-Yueh Yu [a], Ming-Chih Kuo [a], Yuh-Cherng Liou [a,b], Shu-Hua Chien [a,b,*]

[a] Institute of Chemistry, Academia Sinica, Taipei 11529, Taiwan
[b] Department of Chemistry, National Taiwan University, Taipei 10617, Taiwan

ARTICLE INFO

Article history:
Received 25 December 2007
Received in revised form 26 February 2008
Accepted 17 March 2008
Available online 22 March 2008

Keywords:
Titania-nanotube
Pt catalyst
CO_2-TPD/MS
CO_2 hydrogenation

ABSTRACT

The titania-nanotube-supported Pt (Pt/Tnt) catalyst was prepared by the photochemical deposition of Pt complex on the titania-nanotube (Tnt) synthesized by the alkaline hydrothermal method. The physicochemical properties of Pt/Tnt catalyst were investigated by scanning electron microscopy, transmission electron microscopy, X-ray diffraction, N_2 adsorption and desorption isotherms, temperature-programmed reduction and X-ray photoelectron spectroscopy. The Pt/Tnt catalyst exhibited mixed-valence Pt nanoparticles (1–3 nm) dispersed uniformly on the surface of Tnt with a Brunauer–Emmett–Teller surface area of 187 m^2/g. The results of the temperature-programmed desorption of CO_2 indicated the CO_2 adsorption capacity of Tnt was highly enhanced by the supported Pt nanoparticles. *In situ* Fourier-transform infrared spectroscopy demonstrated that the Pt/Tnt catalyst was highly active for the CO_2 hydrogenation toward methane production at relatively low temperature of 100 °C.

1. Introduction

Titania (TiO_2) has received considerable attention in heterogeneous catalysis due to its high chemical stability, high photoactivity, nontoxicity and low cost, and is used in many applications such as environmental remediation, chemical synthesis and energy production and storage [1–10]. Hydrogenation of CO_2 [11–14] and CO [14–17] over TiO_2-supported noble metal catalysts have been intensively studied. Since Iijima [18] discovered carbon nanotubes in 1991, one-dimensional nanomaterials, including oxide nanotubes, have attracted extensive attention due to their nanotubular morphologies and high surface areas. Many synthesis methods for titania-nanotube have been reported, including the electrodeposition (replicated) process using porous anodic-alumina as a template [19,20], the sol–gel template process using self-assembled organic surfactant as a template [21–23], anodization of Ti foil [24,25] and the alkaline hydrothermal method [26,27]. Among them, the alkaline hydrothermal method reported by Kasuga et al. [26,27] is relatively simple and can convert several grams of TiO_2 powder to titania-nanotube. Several research groups [12,28–44] have reported the synthesis of titania-nanotubes by modifying Kasuga's process. Due to the unique morphology and high surface area of titania-nanotube, it exhibited promising applications such as gas adsorbent [38,39] and catalyst supports [12,40–44].

In our preliminary study, we converted the commercial TiO_2 particles to titania-nanotubes (Tnts) by modifying Kasuga's method and then uniformly immobilized Pt nanoparticles on the titania-nanotubes by photochemical deposition (PCD) method [12]. Herein, we will report the detailed physicochemical properties of the Pt/Tnt catalyst. Since methane signals were accidentally detected in the activation process of the Pt/Tnt in hydrogen, we also systematically investigated the adsorption capability and the hydrogenation of CO_2 over Pt/Tnt using temperature-programmed desorption/mass spectrometry (TPD/MS) as well as *in situ* Fourier-transform infrared spectroscopy (*in situ* FT-IR). The Pt/Tnt is a potential catalyst for application in the CO_2 recycling and methane production.

2. Experimental methods

2.1. Preparation of titania-nanotube and Pt/titania-nanotube

Titania-nanotube was prepared by the hydrothermal method. Briefly, 5 g of anatase TiO_2 powder (Merck, Art. 808) was added into a perfluoroalkoxy (PFA) bottle containing 180 mL of 10 M NaOH and stirred for 30 min to form a suspension. The suspension was placed in a Teflon-lined stainless steel autoclave and heated at 110 °C for 90 h. The resultant precipitate was retrieved by centrifugation and rinsed with 0.1 M HCl until the pH value of the eluate reached around 7. Then the collected precipitate was

* Corresponding author at: Institute of Chemistry, Academia Sinica, Taipei 11529, Taiwan. Tel.: +886 2 2789 8528; fax: +886 2 2783 1237.
E-mail address: chiensh@gate.sinica.edu.tw (S.-H. Chien).

0926-3373/$ – see front matter © 2008 Elsevier B.V. All rights reserved.
doi:10.1016/j.apcatb.2008.03.009

dried in an oven at 110 °C overnight. 2 wt% Pt/Tnt was prepared by the PCD method [12,17]. Appropriate amounts of hexachloroplatinic acid ($H_2PtCl_6{\cdot}6H_2O$) and Tnt were mixed in deionized distilled water (resistance > 18 MΩ) in a pyrex beaker. After deaerating by flowing argon (30 mL/min), the sample was irradiated by 350-nm UV lamps for 4 h ($(1.5–5) \times 10^{16}$ photons/(cm^3 s)) in a Rayonet Photochemical Reactor (model RPR-100). The resulted catalyst was collected by centrifugation, rinsed with deionized distilled water, and dried in an oven at 110 °C overnight. 2 wt% Pt/TiO_2 was also prepared by the same procedure using TiO_2 powders (Merck, Art. 808) as the supporting material for a comparative study.

2.2. Sample characterization

The field-emission scanning electron microscopy (FE-SEM), high-resolution transmission electron microscopy (HRTEM) and field-emission transmission electron microscopy (FE-TEM) images of the prepared samples were recorded by a LEO 1530 microscope, a JEOL 2011 microscope and a JEOL JEM-2100 microscope, respectively. The energy dispersive X-ray (EDX) analysis facility in conjunction with the LEO 1530 field-emission scanning electron microscope was used to analyze the chemical composition of the sample. The nitrogen adsorption and desorption isotherms of the catalysts were carried out at −196 °C using a Micromeritics ASAP 2010 Analyzer for the determination of Brunauer–Emmett–Teller (BET) surface area and pore size distribution. The Barrett–Joyner–Halenda (BJH) pore size distribution was obtained according to the desorption isotherm. The Horvath–Kawazoe (HK) method was used to determine the micropore size distribution. The X-ray diffraction (XRD) patterns were recorded by a Siemens D5000 diffractometer equipped with a Cu Kα X-ray source (λ = 1.5405 Å), operating under a voltage of 40 kV and a current of 30 mA. X-ray photoelectron spectroscopy (XPS) was investigated on an Omicron ESCA spectrometer with a monochromatic Al Kα X-ray source. All spectra were calibrated by the C 1s spectrum at 284.5 eV.

2.3. Temperature-programmed techniques

The reducibility of the catalysts was investigated by the temperature-programmed reduction (TPR). In the TPR experiments, 25 mg of the as-prepared catalyst was heated in a flow of 10% H_2/Ar gas mixture (25 mL/min). The heating rate of 10 °C/min was controlled by a WEST 2500 temperature programmer. The amount of H_2 consumption in the reduction of the catalyst was recorded with a thermal conductivity detector built in an Agilent model 6890 N gas chromatograph.

The gas-desorption properties of the catalysts were investigated by a temperature-programmed desorption (TPD) system. In the TPD experiments, 25 mg of catalyst sample was placed in a pyrex tube, which was evacuated to 2×10^{-4} Torr at room

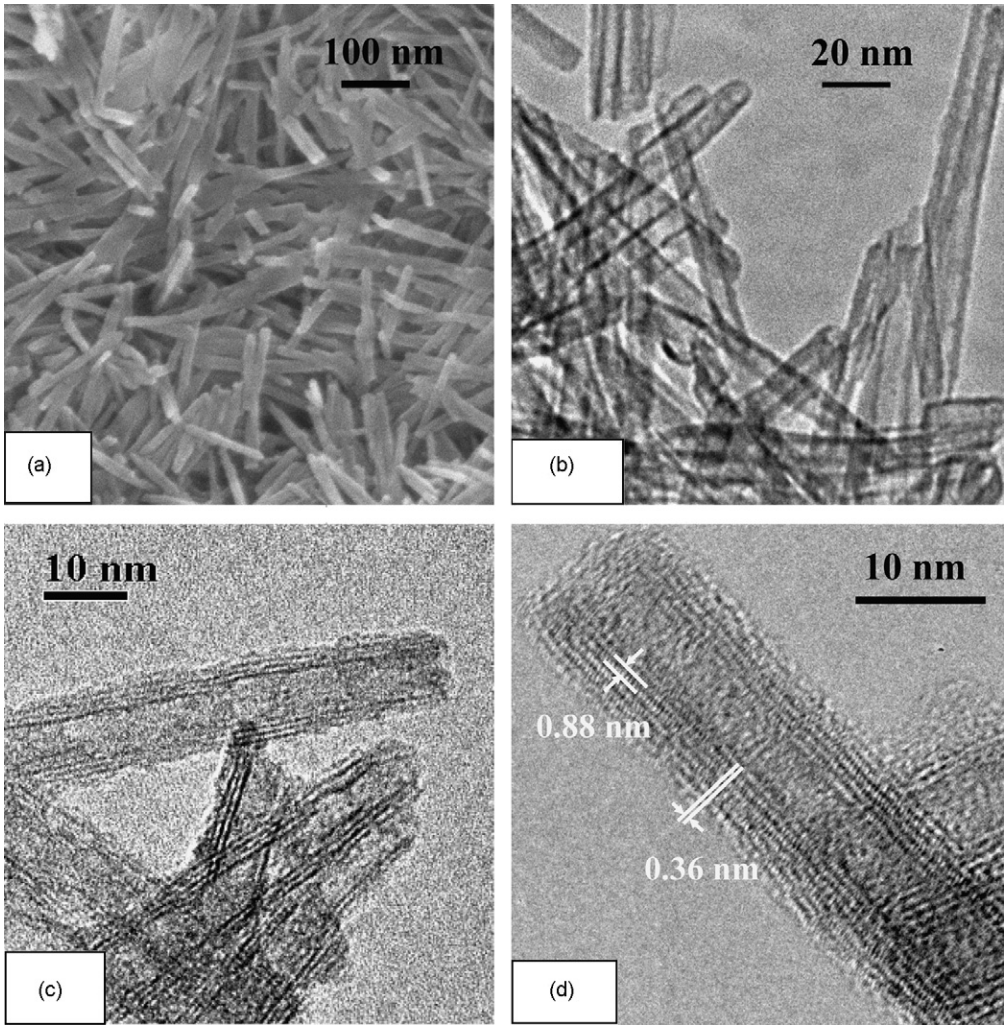

Fig. 1. Electron microscopy images of titania-nanotube (Tnt). (a) FE-SEM, (b) TEM (c) HR-TEM and (d) FE-TEM.

temperature prior to the TPD process. The heating rate of 10 °C/min was controlled by a temperature programmer (WEST 4400). A Hiden HALO 301 quadrupole mass spectrometer was used to simultaneously analyze the desorbed CO_2 ($m/z = 44$).

2.4. In situ FT-IR spectroscopic measurements

In the *in situ* FT-IR spectroscopic measurements, 25 mg of the as-prepared catalyst was dried in an oven at 120 °C for 30 min and then pressed into a self-supporting wafer of 20-mm diameter by applying 10-tons pressure. The catalyst wafer was placed in a quartz IR cell equipped with two KBr windows [17]. The IR cell was immediately evacuated to 2×10^{-4} Torr, and then 60 Torr of H_2 was introduced into the cell. Then, the IR cell was heated in a heating rate of 5 °C/min controlled by a WEST 2500 temperature programmer. While the sample was being heated, the infrared spectra were taken *in situ* on a Bomem DA-8 FT-IR spectrometer operating under evacuated mode.

3. Results and discussion

3.1. Characterization of Tnt and Pt/Tnt

Fig. 1(a) shows the FE-SEM image of the prepared Tnt. The length of randomly tangled Tnt was ranged from 100 nm to several hundred nanometers. The open-end feature of the Tnt with outer diameters in the range of 9–12 nm and inner diameters in the range of 3–5 nm can be observed from the TEM micrographs as shown in Fig. 1(b)–(d). The multi-walled tubular structure with a wall-thickness of 3–4 nm was clearly observed, as shown in Fig. 1(c) and (d). The space between the two adjacent layers of the wall was about 0.88 nm. Each layer of the tubular walls contained periodic lattice fringes with a spacing of about 0.36 nm, as presented in Fig. 1(d). Chen et al. [29] and Bavykin et al. [39] proposed that these lattice fringes were resulted from the zigzag structure of titania-nanotube prepared by alkaline hydrothermal method. Wu et al. [28] demonstrated that these fringes were assigned to the (0 1 0) plane of the monoclinic $H_2Ti_3O_7$. Fig. 2 shows the FE-TEM micrograph Pt/Tnt, after being reduced with H_2 at 200 °C for 1 h. Accordingly, the Pt particles with diameter of 1–3 nm was dispersed uniformly on the surface of Tnt. The deposition of Pt nanoparticles did not significantly affect the tubular feature of the Tnt support.

Fig. 3(a) illustrates the weak XRD profile of Tnt. It is very much different from the diffraction pattern of the parent TiO_2 (Fig. 3(b)) which consisted of a major anatase phase and a trace of rutile phase. Two XRD peaks of Tnt could be identified: the one at $2\theta = 9.9°$ ($d = 0.88$ nm as determined by the Bragg's law $\lambda = 2d \sin\theta$) was due to the space between the scrolled multi-layers, and the peak at $2\theta = 24.5°$ corresponded to the periodic lattice fringes with a 0.36 nm-spacing. The results above were consistent with the observation in the FE-TEM image shown in Fig. 1(d). According to Chen et al. [29], the XRD peak at ca. $2\theta = 29°$ and 48° represent diffraction peaks of the (2 1 1) and (0 2 0) planes of monoclinic $H_2Ti_3O_7$, respectively. Various chemical structure of titania-nanotubes prepared by alkaline hydrothermal method had been proposed, such as $H_2Ti_3O_7$ [28,29,39], $H_2Ti_2O_5{\cdot}H_2O$ [33], $H_2Ti_4O_9{\cdot}H_2O$ [34], $H_xTi_{2-x}\square_{x/4}O_4$ ($x \sim 0.7$ and $\square$ = vacancy) [35], or $Na_xH_{2-x}Ti_3O_7$ ($x \sim 0.75$) [36], according to the XRD results. Although this topic is still under debate, the scrolled mutli-walled nanotubular structure of Tnt is evident.

Fig. 4 shows the N_2 adsorption and desorption isotherms of Tnt at −196 °C. A hysteresis loop appearing at $P/P^0 > 0.5$ was most likely to be attributed to the aggregation of Tnt [36,37]. The BET surface area of Tnt was 191 m^2/g, which was increased by a factor

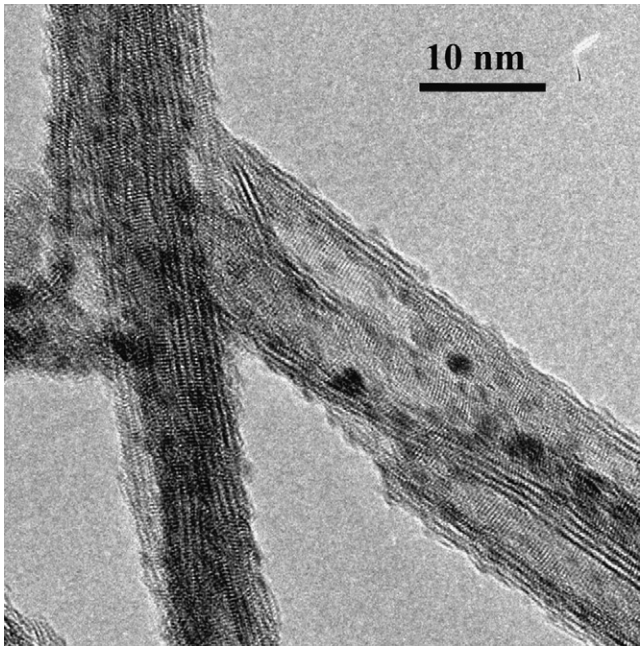

Fig. 2. FE-TEM micrograph of Pt/Tnt.

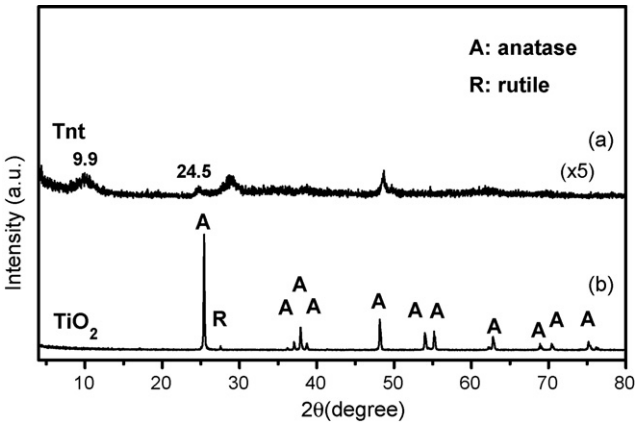

Fig. 3. XRD patterns of (a) Tnt and (b) TiO_2.

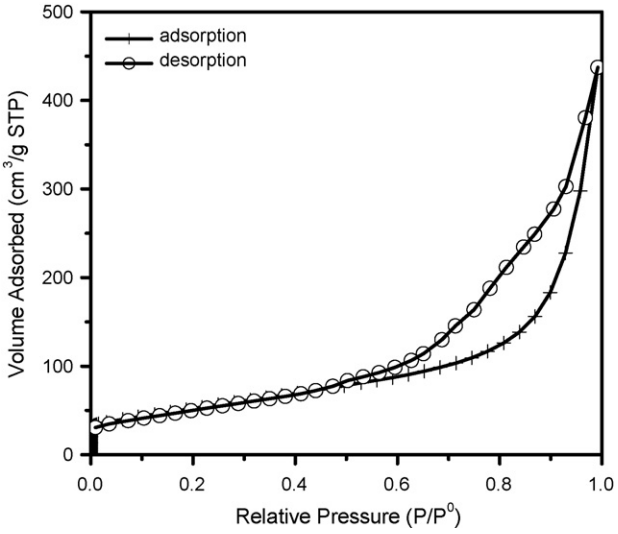

Fig. 4. N_2 adsorption and desorption isotherms of Tnt at −196 °C.

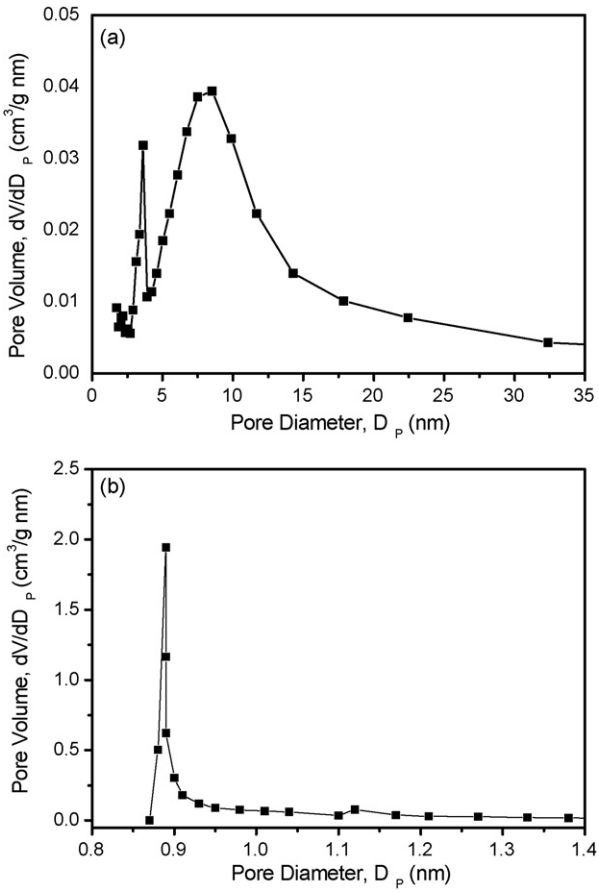

Fig. 5. The pore size distribution of Tnt determined by (a) the BJH and (b) the HK method.

of 38 as compared to the parent TiO_2 (5 m^2/g), and only slightly decreased upon the deposition of Pt (187 m^2/g for Pt/Tnt). Fig. 5(a) exhibits the BJH pore size distribution of Tnt according to the desorption isotherm. Two types of mesoporous structure are depicted in Fig. 5(a). The sharp peak of 3.7 nm was correlated to the inner diameter of Tnt which was consistent with the TEM observation. The broad peak with the pore diameter ranged from 5 to 20 nm was derived from the hysteresis loop ascribed to the aggregation of Tnt [36,37]. The HK pore size distribution shown in Fig. 5(b) revealed a sharp peak at 0.89 nm which was close to the *d* spacing (=0.88 nm) determined from the XRD peak at $2\theta = 9.9^\circ$ and the layer spacing observed in the TEM micrograph.

As shown in Fig. 6, the TPR profile of the Pt/Tnt catalyst exhibited a sharp H_2 consumption peak at 103 °C, which was ascribed to the reduction of the non-zero-oxidation state platinum deposited on the as-prepared Pt/Tnt catalyst. A shoulder was clearly observed at the right-hand side of this reduction peak, implying that the Pt nanoparticles over Pt/Tnt would be in mixed-valance states. In the TPR profile of the as-prepared Pt/TiO_2, no reduction peak for non-metallic Pt was observed. It indicated that the Pt particles on the PCD-prepared Pt/TiO_2 were mostly in the metallic state, Pt^0. The mixed-oxidation states of the platinum on the Tnt and TiO_2 can also be indicated by the color of the as-prepared samples. The dark gray color of Pt/TiO_2 indicated that most of the platinum was metallic, while the yellowish light gray color of Pt/Tnt implied that some non-metallic platinum retained on the surface of Tnt. Moreover, a broad peak at higher temperature with maximum at 364 and 397 °C in the TPR profiles of the as-prepared Pt/TiO_2 and Pt/Tnt, respectively, was attributed

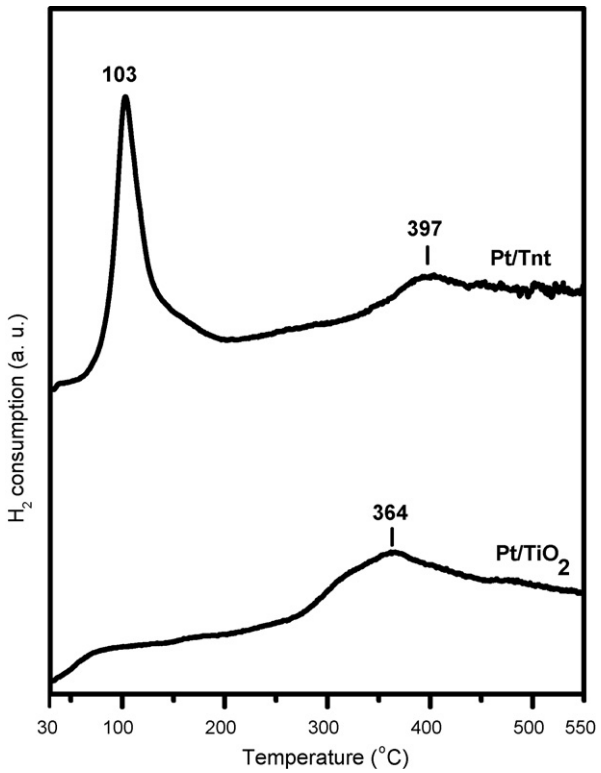

Fig. 6. TPR profiles of Pt/Tnt and Pt/TiO_2.

to the partial reduction of TiO_2 and Tnt by hydrogen upon the metal–support interaction [45]. This H_2 consumption peak of Pt/TiO_2 was remarkably larger than that of Pt/Tnt. It implied that the metal–support interaction between Pt and TiO_2 was more pronounced than the interaction between Pt and Tnt.

The chemical states of Pt nanoparticles on Pt/Tnt were investigated and confirmed by XPS. Fig. 7 shows the deconvolution results of Pt 4f spectra of the as-prepared Pt/Tnt. The binding energies of Pt $4f_{7/2}$ electron at 71.6, 73.0 and 74.5 eV were attributed to Pt^0, Pt^{2+} and Pt^{4+}, respectively [46]. Accordingly, the Pt/Tnt contained mainly Pt^{2+} (60%), some Pt^{4+} (30%), and a few Pt^0 (10%). On the other hand, the XPS results of the Pt/TiO_2 showed that the chemical states of platinum were mainly Pt^0, with less than 15% of Pt^{2+}.

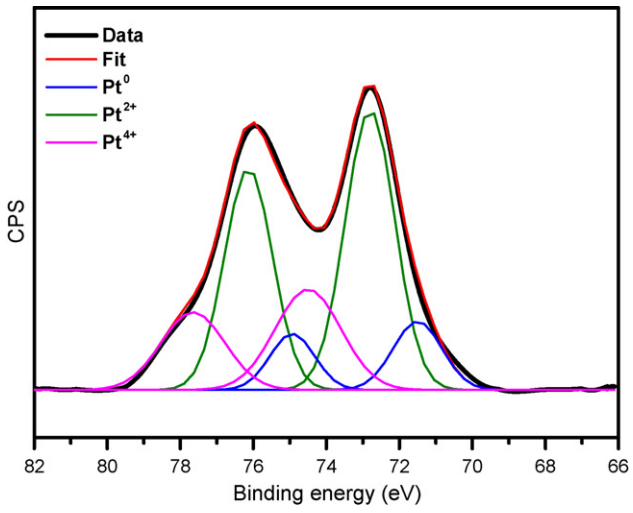

Fig. 7. The deconvolution of Pt 4f XPS spectrum of the as-prepared Pt/Tnt.

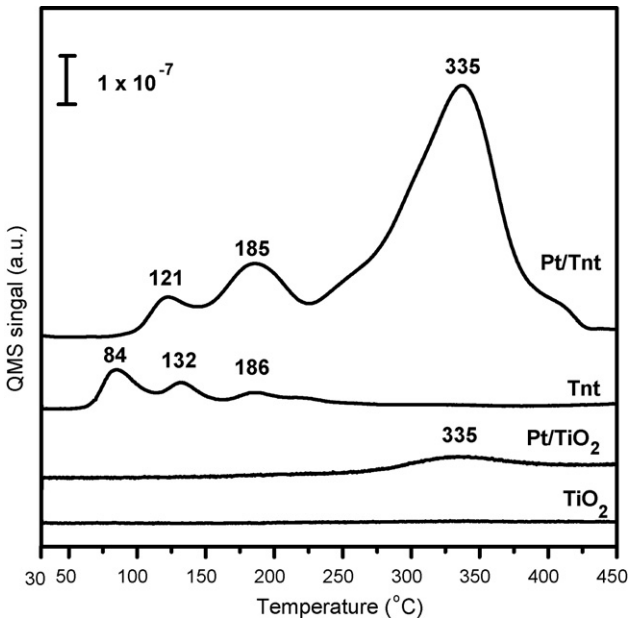

Fig. 8. CO_2-TPD profiles of TiO_2, Pt/TiO_2, Tnt and Pt/Tnt.

3.2. TPD/MS studies of Pt/Tnt and Pt/TiO_2

In order to investigate the CO_2 adsorption capacity of these samples, the TPD of CO_2 from Tnt, TiO_2, Pt/Tnt and Pt/TiO_2 were performed, and the results are illustrated in Fig. 8. As shown in the CO_2-TPD profile of TiO_2, there was almost no CO_2 desorbed from TiO_2, indicating that no CO_2 was adsorbed on the TiO_2 powder. The CO_2-TPD profile of Pt/TiO_2 showed a weak CO_2 desorption peak with maximum at 335 °C, implying that the Pt particles on the TiO_2 could induce a certain extent of the CO_2 adsorption. The effect of Pt might result from the dissociative adsorption of CO_2 on the titania-supported Pt [47,48].

In the CO_2-TPD profile of Tnt, three distinguished desorption peaks appeared with maxima at 84, 132 and 186 °C, which might be due to the CO_2 desorption from the mesopores resulted from the aggregation of Tnt (pore diameter 5–20 nm), the inner pore of Tnt (pore diameter 3–4 nm) and the interlayer space (pore diameter = 0.89 nm), respectively. Both the high surface area and the unique tubular morphology of Tnt resulted in the enhancement of CO_2 adsorption. Besides, the residual sodium in the Tnt as evidenced by EDX with Na/Ti atomic ratio of 0.01 might be also responsible for the CO_2 adsorption [49]. Onishi and Iwasawa [50] demonstrated that the presence of Na adatoms, which added the basicity of the substrate, enhanced the chemisorption of CO_2 on TiO_2 surface due to a typical acid–base surface reaction.

The peaks appeared at 121 and 185 °C in the CO_2-TPD profile of Pt/Tnt might correspond to the CO_2 desorption from the aggregate mesopores and the inner pores of Pt/Tnt. There was also a large peak at 335 °C that is related to the CO_2 desorption from the mixed-valence Pt nanoparticles. In a similar CO_2-TPD experiment carried out for the Pt/Tnt pretreated with H_2 at 200 °C for 1 h, the desportion peak at 335 °C was almost undetectable. The higher CO_2 desorption temperatures of Pt/Tnt as compared to those of Tnt were due to the stronger adsorption of CO_2 on the Pt/Tnt. The larger CO_2 desoption peaks from the Pt/Tnt catalyst as compared to those from the Tnt indicates that the capacity of CO_2 adsorption on the Pt/Tnt catalyst was highly enhanced by the deposited mixed-valence Pt nanoparticles.

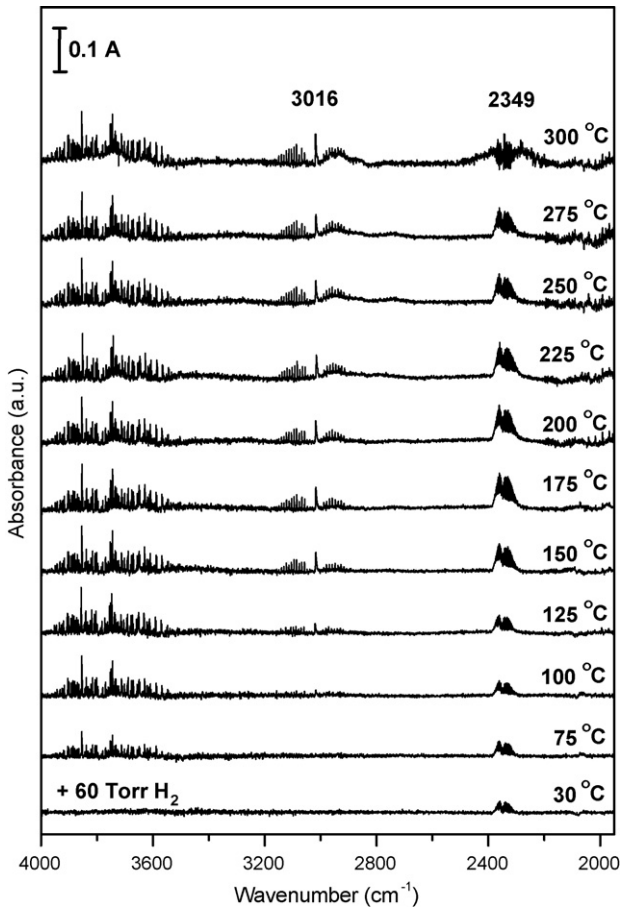

Fig. 9. *In situ* FT-IR spectra of the as-prepared Pt/Tnt catalyst placed in a preevacuated IR cell heating from 30 to 300 °C at 5 °C/min in 60 Torr H_2.

3.3. In situ FT-IR studies of CO_2 hydrogenation over Pt/Tnt and Pt/TiO_2

Fig. 9 shows the *in situ* FT-IR spectra of Pt/Tnt being heated at a rate of 5 °C/min in 60 Torr H_2. The *in situ* FT-IR spectra of Pt/TiO_2 were also recorded for a comparative study, as shown in Fig. 10. The variations of the signal intensities in Figs. 9 and 10 are depicted in Fig. 11(a) and (b), respectively. In the case of Pt/Tnt, the signals of gaseous CO_2 (2349 cm^{-1}) appeared at 30 °C upon the introduction of H_2 gas. Since there was no leakage in the system, the CO_2 signals seemed to be resulted from the weakly adsorbed CO_2 that was repelled by H_2 due to a competitive adsorption between H_2 and CO_2 on the Pt/Tnt surface. The signals of gaseous CH_4 (3016 cm^{-1}) appeared at a relatively low temperature of 100 °C. The intensity of gaseous CH_4 band increased gradually with raising temperature and reached a plateau at 175 °C, as shown in Fig. 11(a). The mechanism of methanation of CO_2 with H_2 was similar to that over ruthenium-supported TiO_2 catalyst (the Sabatier reaction) [11] as the following equation:

$$CO_{2\,ad} + 8H_{ad} \rightarrow CH_4 + 2H_2O$$

The intensity of H_2O signals in Fig. 9 increased with temperature and achieved a plateau at 125 °C. The H_2O signals were contributed partially to the dehydration of Tnt support and partially to the H_2O formation from the reduction of Pt oxides by H_2 and CO_2 hydrogenation. Beside the water signals at 1634 cm^{-1}, no significant spectrum variation was observed below 2100 cm^{-1}. The direct formation of CH_4 from CO_2 hydrogenation was addressed.

In the case of Pt/TiO_2, the *in situ* FT-IR spectra as depicted in Fig. 10 showed a quite different phenomenon. There was no CO_2

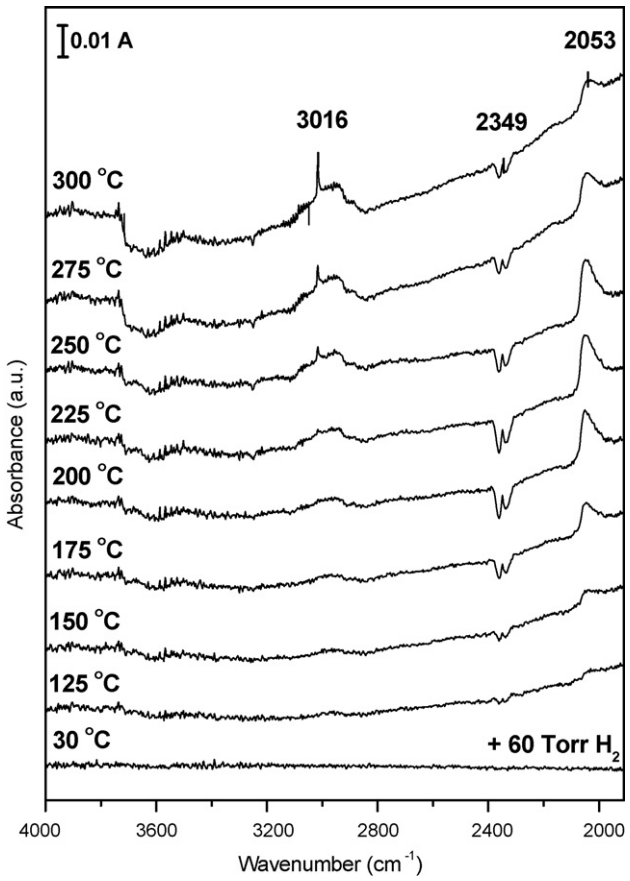

Fig. 10. *In situ* FT-IR spectra of the as-prepared Pt/TiO_2 catalyst placed in a preevacuated IR cell heating from 30 to 300 °C at 5 °C/min in 60 Torr H_2.

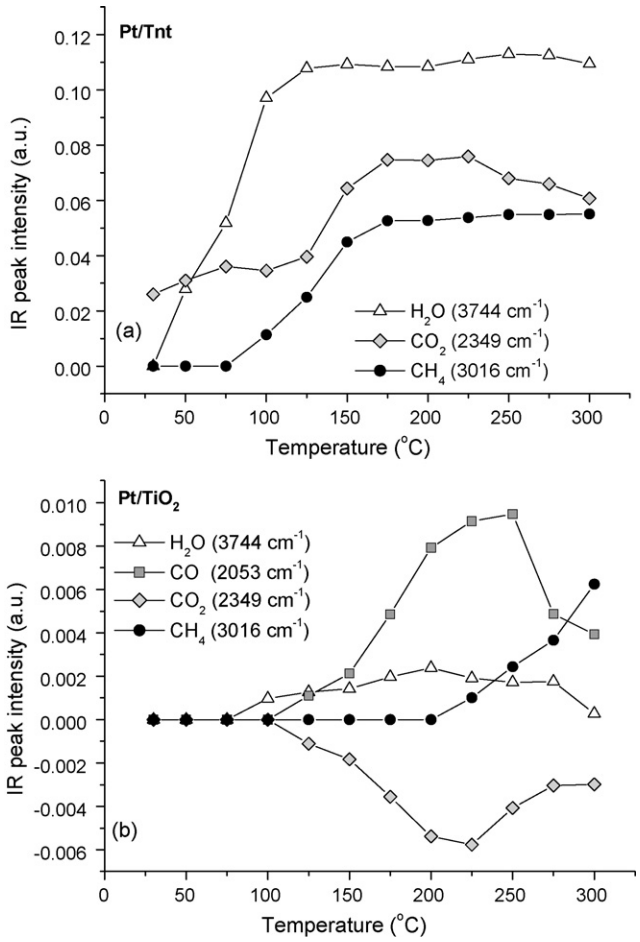

Fig. 11. Variations of *in situ* FT-IR signal intensities with temperature raising (a) Pt/Tnt and (b) Pt/TiO_2.

signal appearing upon the introduction of H_2 at room temperature. It implied that there was no weakly adsorbed CO_2 as evidenced by the results of CO_2-TPD. Negative CO_2 vibration bands centered at 2349 cm^{-1} was possibly due to the consumption of the residual CO_2 after the evacuated process, since the *in situ* FT-IR experiment was not conducted in an ultra-high vacuum system. The CO_2 negative band started appearing at temperature above 125 °C and increased progressively with temperature increasing up to 225 °C, as shown in Fig. 11(b). Simultaneously, a 2053 cm^{-1} band appeared at temperature above 125 °C which represented the CO linearly adsorbed on the well-dispersed Pt sites [17,48,51]. The adsorbed CO was generated possibly by the dissociative adsorption of CO_2 on Pt/TiO_2 [47,48]:

$$CO_2 \rightarrow CO_{ad} + O_{ad}$$

or by the reduction of CO_2 with H_2 to produce CO and H_2O via reverse water–gas shift reaction [13,52,53]:

$$CO_2 + 2H_{ad} \rightarrow CO_{ad} + H_2O$$

The signals of gaseous methane (3016 cm^{-1}) appeared as the temperature reached 225 °C, and the intensity of the signals increased with the temperature increasing. The mechanism of methanation could be expressed as the following equation:

$$CO_{ad} + 6H_{ad} \rightarrow CH_4 + H_2O$$

Moreover, the consumption of adsorbed carbonate (1630 and 1375 cm^{-1}) [54] along with the formation of formic acid (788, 1363, 2951 and 3524 cm^{-1}) occurring simultaneously was observed in the spectra below 2000 cm^{-1} as temperature higher than 100 °C (not shown here) according to:

$$CO_{3\,ad}{}^{2-} + 2H_{ad} \rightarrow HCOOH + O^{2-}{}_{ad}$$

According to the *in situ* FT-IR results, CO_2 can undergo catalytic hydrogenation to give CH_4 *via* the intermediate of CO over Pt/TiO_2 catalyst. Other than CH_4, HCOOH was also found as a by-product. Without finding other product except for CH_4, the excellent catalytic activity of Pt/Tnt catalyst for CO_2 hydrogenation is superior to that of Pt/TiO_2.

4. Conclusions

A unique titania-nanotube-supported platinum (Pt/Tnt) catalyst was prepared. The catalyst, with a high surface area of 187 m^2/g, is a scrolled multi-walled titania-nanotubing uniformly dispersed with Pt nanoparticles (about 1–3 nm) that are in the mixed-valence states as demonstrated by TPR and XPS. The CO_2-TPD results indicated that a large amount of CO_2 adsorbed on the Pt/Tnt. The high CO_2 adsorption capacity of Pt/Tnt was ascribed to the synergetic effect of the high surface area tubular morphology and the mixed-valence Pt nanoparticles. The *in situ* FT-IR manifested that the Pt/Tnt was a highly active catalyst for the CO_2 hydrogenation toward methane production at a relatively low temperature of 100 °C. Conclusively, the Pt/Tnt can be a potential catalyst for CO_2 recycling and methane production.

Acknowledgment

The financial supports from Academia Sinica and the National Science Council of Taiwan, ROC, are gratefully appreciated. We also acknowledge the Instrumentation Center of National Taiwan University for the FE-SEM measurements and the Institute of Physics, Academia Sinica for recording the FE-TEM.

References

[1] G.N. Kryukova, G.A. Zenkovets, A.A. Shutilov, M. Wilde, K. Günther, D. Fassler, K. Richter, Appl. Catal. B 71 (2007) 169–176.
[2] O. Ozcan, F. Yukruk, E.U. Akkaya, D. Uner, Appl. Catal. B 71 (2007) 291–297.
[3] K.-P. Yu, G.W.M. Lee, Appl. Catal. B 75 (2007) 29–38.
[4] E.A. Kozlova, A.V. Vorontsov, Appl. Catal. B 77 (2007) 35–45.
[5] C. Young, T.M. Lim, K. Chiang, J. Scott, R. Amal, Appl. Catal. B 78 (2008) 1–10.
[6] Y. Ishibai, J. Sato, T. Nishikawa, S. Miyagishi, Appl. Catal. B 79 (2008) 117–121.
[7] M.R. Hoffmann, S.T. Martin, W. Choi, D.W. Bahnemann, Chem. Rev. 95 (1995) 69–96.
[8] D.V. Bavykin, J.M. Friedrich, F.C. Walsh, Adv. Mater. 18 (2006) 2807–2824.
[9] I.K. Konstantinou, T.A. Albanis, Appl. Catal. B 42 (2003) 319–335.
[10] A. Hagfeldt, M. Grätzel, Chem. Rev. 95 (1995) 49–68.
[11] K.R. Thampi, J. Kiwi, M. Grätzel, Nature 327 (1987) 506–508.
[12] S.H. Chien, Y.C. Liou, M.C. Kuo, Synth. Met. 152 (2005) 333–336.
[13] H. Sakurai, M. Haruta, Catal. Today 29 (1996) 361–365.
[14] H. Sakurai, M. Haruta, Appl. Catal. A 127 (1995) 93–105.
[15] M.A. Vannice, C. Sudhakar, J. Phys. Chem. 88 (1984) 2429–2432.
[16] T. Mori, S. Taniguchi, Y. Mori, T. Hattori, Y. Murakami, J. Catal. 108 (1987) 501–502.
[17] S.H. Chien, K.N. Lu, C.T. Chen, Bull. Inst. Chem. Acad. Sin. 40 (1993) 37–46.
[18] S. Iijima, Nature 354 (1991) 56–58.
[19] S.M. Liu, L.M. Gan, L.H. Liu, W.D. Zhang, H.C. Zeng, Chem. Mater. 14 (2002) 1391–1397.
[20] P. Hoyer, Langmuir 12 (1996) 1411–1413.
[21] B.B. Lakshmi, C.J. Patrissi, C.R. Martin, Chem. Mater. 9 (1997) 2544–2550.
[22] S. Kobayashi, K. Hanabusa, N. Hamasaki, M. Kimura, H. Shirai, Chem. Mater. 12 (2000) 1523–1525.
[23] J.H. Jung, H. Kobayashi, K.J.C. van Bommel, S. Shinkai, T. Shimizu, Chem. Mater. 14 (2002) 1445–1447.
[24] D. Gong, C.A. Grimes, O.K. Varghese, W. Hu, R.S. Singh, Z. Chen, E.C. Dickey, J. Mater. Res. 16 (2001) 3331–3334.
[25] C.J. Lin, W.Y. Yu, S.H. Chien, Appl. Phys. Lett. 91 (2007) (Article No. 233120).
[26] T. Kasuga, M. Hiramatsu, A. Hoson, T. Sekino, K. Nihara, Langmuir 14 (1998) 3160–3163.
[27] T. Kasuga, M. Hiramatsu, A. Hoson, T. Sekino, K. Nihara, Adv. Mater. 11 (1999) 1307–1311.
[28] D. Wu, J. Liu, X. Zhao, A. Li, Y. Chen, N. Ming, Chem. Mater. 18 (2006) 547–553.
[29] Q. Chen, G.H. Du, S. Zhang, L.-M. Peng, Acta Crystallogr. Sect. B: Struct. Sci. 58 (2002) 587–593.
[30] C.H. Lin, S.H. Chien, J.H. Chao, C.Y. Sheu, Y.C. Cheng, Y.J. Huang, C.H. Tsai, Catal. Lett. 80 (2002) 153–159.
[31] D.S. Seo, J.K. Lee, H. Kim, J. Cryst. Growth 229 (2001) 428–432.
[32] B.D. Yao, Y.F. Chan, X.Y. Zhang, W.F. Zhang, Z.Y. Yang, N. Wang, Appl. Phys. Lett. 82 (2003) 281–283.
[33] C.-C. Tsai, H. Teng, Chem. Mater. 18 (2006) 367–373.
[34] A. Nakahira, W. Kato, M. Tamai, T. Isshiki, K. Nishio, H. Aritani, J. Mater. Sci. 39 (2004) 4239–4245.
[35] R. Ma, K. Fukuda, T. Sasaki, M. Osada, Y. Bando, J. Phys. Chem. B 109 (2005) 6210–6214.
[36] X. Sun, Y. Li, Chem. Eur. J. 9 (2003) 2229–2238.
[37] C.-C. Tsai, J.-N. Nian, H. Teng, Appl. Surf. Sci. 253 (2006) 1898–1902.
[38] S.H. Lim, J. Luo, Z. Zhong, W. Ji, J. Lin, Inorg. Chem. 44 (2005) 4124–4126.
[39] D.V. Bavykin, A.A. Lapkin, P.K. Plucinski, J.M. Friedrich, F.C. Walsh, J. Phys. Chem. B 109 (2005) 19422–19427.
[40] V. Idakiev, Z.-Y. Yuan, T. Tabakova, B.-L. Su, Appl. Catal. A 281 (2005) 149–155.
[41] D.V. Bavykin, A.A. Lapkin, P.K. Plucinski, J.M. Friedrich, F.C. Walsh, J. Catal. 235 (2005) 10–17.
[42] C.-C. Tsai, H. Teng, Chem. Mater. 16 (2004) 4352–4358.
[43] T. Akita, M. Okumura, K. Tanaka, K. Ohkuma, M. Kohyama, T. Koyanagi, M. Daté, S. Tsubota, M. Haruta, Surf. Interface Anal. 37 (2005) 265–269.
[44] B. Zhu, Q. Guo, X. Huang, S. Wang, S. Zhang, S. Wu, W. Huang, J. Mol. Catal. A 249 (2006) 211–217.
[45] P. Panagiotopoulou, A. Christodoulakis, D.I. Kondarides, S. Boghosian, J. Catal. 240 (2006) 114–125.
[46] S.H. Chien, M.C. Kuo, C.H. Lu, K.N. Lu, Catal. Today 97 (2004) 121–127.
[47] K. Tanaka, K. Miyahara, I. Toyoshima, J. Phys. Chem. 88 (1984) 3504–3508.
[48] K. Tanaka, J.M. White, J. Phys. Chem. 86 (1982) 3977–3980.
[49] U. Dieblod, Surf. Sci. Rep. 48 (2003) 53–229.
[50] H. Onishi, Y. Iwasawa, Catal. Lett. 38 (1996) 89–94.
[51] V.A. Self, P.A. Sermon, J. Phys.: Condens. Matter 1 (1989) SB221–SB224.
[52] A. Goguet, F. Meunier, J.P. Breen, R. Burch, M.I. Petch, A.F. Ghenciu, J. Catal. 226 (2004) 382–392.
[53] H. Sakurai, A. Ueda, T. Kobayashi, M. Haruta, Chem. Commun. (1997) 271–272.
[54] J.M. Pigos, C.J. Brooks, G. Jacob, B.H. Davis, Appl. Catal. A 319 (2007) 45–57.